Periodica Polytechnica Chemical Engineering

60(3), pp. 141-151, 2016
DOI: 10.3311/PPch.8879

RESEARCH ARTICLE

Received 07 December 2015; accepted after revision 08 March 2016

Induction Heating Consolidation of TiO_2 Sol-Gel Coating on Stainless Steel Support for Photocatalysis Applications

Dreidy Vásquez[1*], Oscar Jerez[2], Rodrigo Schrebler[1], Carlos Carlesi[1], Danilo Carvajal[3,4], Nelson Cáceres[5], Ricardo Schrebler[5]

Abstract

A high-frequency induction heater was used to sinter titanium dioxide thin film on stainless steel plates with the aim of being used as photo-electrodes in wastewaters treatment. To validate the use of this sintering technique, the electrodes were prepared using sol-gel and dip-coating, followed by two different annealing processes for comparison: a conventional furnace and a high-frequency induction heating. To characterize the electrodes, X-ray diffraction (XRD), scanning electron microscopy (SEM) and electrochemical and photocatalysis tests were performed. Anatase and rutile phases were obtained for both annealing techniques. A more regular surface morphology was achieved via the induction heating (IH) treatment at 300 ºC. The impedance study showed a lower resistance of IH samples, representing an improvement in the charge carrier separation and its fast transfer to the surface of the electrode. The photo-oxidation of methylene blue exhibited a higher degradation compared with the conventional furnace samples prepared in this study.

Keywords

Induction heating sintering, Electrochemical techniques, Coatings, Titanium dioxide, Photocatalysis, Azo dye

[1] Pontificia Universidad Católica de Valparaíso, Escuela de Ingeniería Química, Av. Brasil 2950, Valparaíso 2340025, Chile

[2] Universidad de Concepción, Instituto de Geología Económica Aplicada, GEA, Concepción, Chile

[3] Centro de Investigación Tecnológica del Agua en el Desierto (CEITSAZA), Universidad Católica del Norte, Av. Angamos 0610, Antofagasta 1270709, Chile

[4] International Organization for Dew Utilization (OPUR), 60 rue Emeriau, Paris 75015, France

[5] Pontificia Universidad Católica de Valparaíso, Facultad de Ciencias, Avda. Universidad 330, Valparaíso, Chile

[*] Corresponding author, e-mail: dreidy.vasquez@ucv.cl

1 Introduction

The remission of toxic contaminants and the use of clean energy, such as the energy of the sun, for this purpose have become popular topics for many research teams. The development of any nation in the world demands a better and major use of energy that must be efficient and have a low environmental impact. Wastewater treatment via an advanced oxidation process, which uses toxic elements from organic sources, is one of the aims of photocatalysis. The process has a high efficiency for neutralizing these toxic compounds and presents the opportunity to produce electrodes that are compatible with the environment [1]. The capability of the electrodes, chemistry process, associated cost effects and the product lifetime are related to the type of material used, and to its structure, stability, and porosity, the substrate material and shape, and the successful adhesion of the coating. These factors must be improved to reach a massive industrial application of this process. Many other factors can affect the stability of the electrode, such as substrate preparation (in particular with metallic support), the inclusion of a dopant, the solvent involved in the synthesis of the electrodes, the preparation methods and the parameters of thermal decomposition (temperature, heating rate and time) [2].

Titanium oxide is one of the most studied materials for photocatalysis applications because it exhibits highly photocatalytic properties and is stable, non-toxic and relatively cheap to produce. The most efficient form of use is via the commercial nanopowders called Degussa P-25 TiO_2 [3]. However, the use of these nanopowders generates secondary costs, associate with the need for a high cost filter system to separate the particles from the treated water. To avoid this problem, studies have been conducted to obtain a material supported by a substrate that can be reused, but it must also withstand the reactor conditions during treatment. Simultaneously, these studies have tried to improve the photocatalytic activity of the material by improving the anatase phase stability, porosity distribution, superficial contact area and other variables [4, 5, 6, 7, 8]. Numerous substrates have been studied and used to fabricated these types of electrodes, including stainless steel, paper, conductive glass, titanium, ceramic foam, TiO_2 nanoneedle/nanoribbon

spheres [9] and a rubber sheet strewn with titanium dioxide particles [10] that can be recovered from the treatment process and reused. Nevertheless, all of these solutions address the difficulty of improving the photocatalytic activity results obtained compared with titanium dioxide nanopowders.

Several technique have been used to coat stainless steel substrate for use as an electrode support, including Chemical Vapour Deposition (CVD), sol-gel, spray pyrolysis, plasma spraying and sputtering [11-14]. In this case, we employed the sol-gel dip coating method because it is a simple technique for obtaining a homogeneous coating, with an effective control of the composition and a mesoporous thin film.

The sintering process is another experimental condition that has a strong effect on the electrochemical properties of these oxides. Decomposition can occur directly via sputtering, plasma spray, spray pyrolysis [12-14] or the standard method, which utilizes a furnace after coating the substrate. In this case, we proposed the use of an electromagnetic induction heater to promote a rapid consolidation of the coating to the substrate. Until now, new studies have used electromagnetic induction heating to sinter thermal oxide for photocatalysis. The first one was Mousty et al. (1999) [2] that fabricate DSA type electrodes using induction heating. They observed an activation process during cycling voltammetry, which was caused by metallic particles that were left within the coating during rapid decomposition. The advantage of this technique was the reduction of the decomposition time, from several hours in a standard oven to 1 s. For other part, Yang et al. (2012) studied the production of thin iron alloy films in a low carbon steel substrate using high frequency induction heating at a temperature below 600 ºC [15]. Induction heating is a phenomenon where a generated electric current is induced by a magnetic field produced by a current fluctuation on a conducted coil [16]. The magnetic field oscillations produced by the AC current induce an eddy current to the Joule effect. These currents cause a loss of Ohmic heat inside the sample. Most of the dissipated heat is produced within a thin film under the surface. The deepness of the effect depends of the frequency of the current, electric conductivity and magnetic permeability [16]. At high frequencies, more current is induced on the surface. During large-scale material production, it is important to balance cost effectiveness, high efficiency and environmental friendliness when developing fabrication techniques. Electromagnetic induction heating incorporates surface heating instead of conventional volume heating. This is advantageous because it provides a rapid heating time and a reduced cooling time, is environmentally friendly and saves energy.

In this study, we use stainless steel (SS) plates coated with titanium dioxide, which was accomplished using a sol-gel dip-coating, and by sintering with an induction heater. To our knowledge, it is the first time that pressureless induction heating has been used to sinter TiO_2 to SS plates. The aim of this sintering technique is to improve the consolidation of the system substrate-coating. The very fine microstructure that this process could give to the composites, based on the results where FAST processes were used, can enhance the photocatalytic properties of the supported oxide, thus making the method ideal for large-scale applications. The aim of this study is to observe the effect of the sintering process on titanium dioxide, evaluate its photocatalytic performance and establish an efficient, low cost, low energy consumption and scalable method for preparing electrodes.

2 Experimental Procedure

2.1 Materials

Titanium (IV) n-butoxide, ($Ti(OBu)_4$), (Sigma-Aldrich reagent, grade 97 %), 2-propanol (Sigma-Aldrich reagent, anhydrous, 99.5 %), acetic acid (ACS reagent, 99.7 %) and deionized water were used to synthesize titanium oxide. Stainless steel AISI 304 plates of 40 x 40 x 0.5 mm were used as substrates. Sulphuric acid (96 %, Fisher) was used to treat the surface of the substrates. Methylene blue AR LobalChemie, as pollutant, and Polyethylene glycol methyl ether Mn5000 (Sigma-Aldrich) were used as the template for the mesoporous structure.

2.2 Synthesis route and sintering methods

The titanium (IV) n-butoxide was dissolved on 83 % 2-propanol slowly, and heated at 50 ºC while it was stirred. To complete the process, the 17 % 2-propanol was mixed with water at a ratio of 1:5. It was then added dropwise while continuously stirring. After obtaining the sol-gel, 2 g of polyethylene glycol were added and stirred for 4 h at 50 ºC. The precursor sol was aged two days at room temperature. The thin film on the stainless steel was dip-coated at a withdraw rate of 2 mm/s and dried at room temperature for 1 h. The sintering process was developed in two ways, for comparison. The first was using a conventional furnace at 600 ºC for 1 h. The second used homemade high-frequency induction heater for 5 min (reaching a temperature of 300 ºC, measured by an optical pyrometer at the center of the substrate plate).

2.3 Microstructure and phase analysis

To study the phase formation, crystal size, and surface morphology of the films, XRD measurements were performed on a D8 Advance Bruker diffractometer, ($CuK\alpha_1$, $\lambda = 1.5406$, and current of −30 mA, COD). The Scherrer equation was used to determine the average diameter of the particles. The surface morphology was analyzed using a Scanning electron microscope SEM JEOL JSM 6380lb.

2.4 Electrochemical Characterization

Electrochemical characterization was analyzed using linear sweep voltammetry (LSW) test with an AUTOLAB. Mott-Schottky measurements (The potential range was −1.2 to 0

$V_{Ag/AgCl}$ at a constant frequency of 1 KHz) and Electrochemical Impedance Spectroscopy (EIS) were conducted in the dark and with UV illumination using a Zahner CIMPS-1. A photochemical Teflon cell with a quartz window was used, including a platinum counter electrode wire and an Ag/AgCl, K_2SO_4 (saturated) reference electrode. The electrolyte solution consisted of 0.1 M potassium sulphate (K_2SO_4) at pH 6.74, at a frequency range of 100 kHz to 100 mHz and a DC potential of 0.2 $V_{Ag/AgCl}$. Corrosion tests were performed on Stainless Steel substrate uncoated and coated by TiO_2, sintered by induction heater and conventional furnace, by polarization measurements on 3.5 wt% of NaCl (pH=5) with the same three electrode cells used for EIS studies. The open circuit potential (OCP) was registered for 1 h and the corrosion parameters were estimated by extrapolation of the Tafel plots.

2.5 Photocatalytic Degradation of Methylene Blue

The photo-degradation of an Azo dye, such as Methylene blue (MB), was carried out in a home-made photocell with 4 UV lamps (20 W power, 365 nm maximum radiation) mounted 10 cm above the center of the double-wall Pyrex glass reactor, which was surrounded by a thermostating jacket (25 ºC). The average UV light intensity inside the photoreactor box was approximately, 606.69 μW/cm^2. This was measured at the center, toward all faces and 3.6 cm from the bottom. The electrode, which had an exposed surface area of 1600 cm^2, was located in the reactor with the 0.01 M methylene blue solution. The solution had its pH adjusted to 10 using 0.1 M NaOH, which was conducted over 2 h to account for adsorption-desorption equilibrium. The measurements were performed for 240 min. Every 20 min, a 5 ml of sample of solution was collected. The degradation of the samples was analyzed using a UV-vis spectrophotometer in a Beckman DU 650 Spectrophotometer at a wavelength scan of 664 nm.

3 Results and Discussion

3.1 Characterization of surface morphology

3.1.1 Pretreatment of substrates for thin film deposition

As shown in Fig. 1a, the stainless steel substrate has a surface morphology that is too smooth to be effectively coated using precursor-sol. Therefore, it is necessary to pretreat the plates. Various processes have been used to increase the surface roughness of the substrate, including mechanical, thermal, chemical or combination treatment techniques [4, 20]. Many researchers prefer to use a combination of thermal and chemical treatments because they significantly increase surface roughness. This study utilized a chemical-thermal treatment with a modification. In general, chemical treatments have durations of 2 or 3 h and the combinations of the two processes have a minimum duration of 24 h. However, this study attempted to provide the same effect without the thermal treatment. Therefore, the plates were left in a sulfuric acid solution (30 wt%) for 8 h, and then rinsed three times with deionized water in ultrasound bath. The result is shown in Fig. 1b. The surface morphology changed from the characteristic grains of an austenitic alloy to a series of pores and ridges. This modified chemical treatment demonstrated that it is possible to significantly increase the roughness of stainless steel samples with only one treatment and in less time.

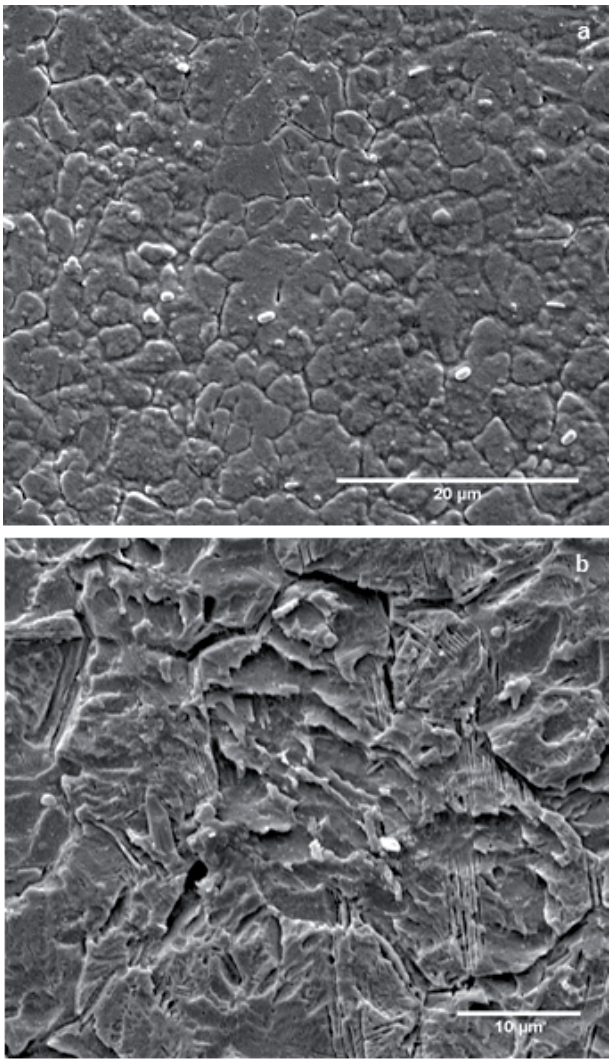

Fig. 1 SEM images of stainless steel substrate: (a) as-received and (b) after chemical etching with H_2SO_4(30%wt.)

3.1.2 Coating Morphology

The main objective of this work is to evaluate the effect of the sintering process using induction heated for titanium dioxide films. Figure 2 illustrates that the sol-gel precursor successfully crystallized for both annealing technique, which included conventional furnace (CF) and induction heating (IH) at atmospheric pressure. In addition, the treated film remained highly porous. The mesoporous thin film consisted of interconnected grain particles with macro-cracks. When previous layers could be seen due to the significant depth of the macro-cracks, the particles were fused together in various spots point to create higher contours differences all over the film. In the case of IH

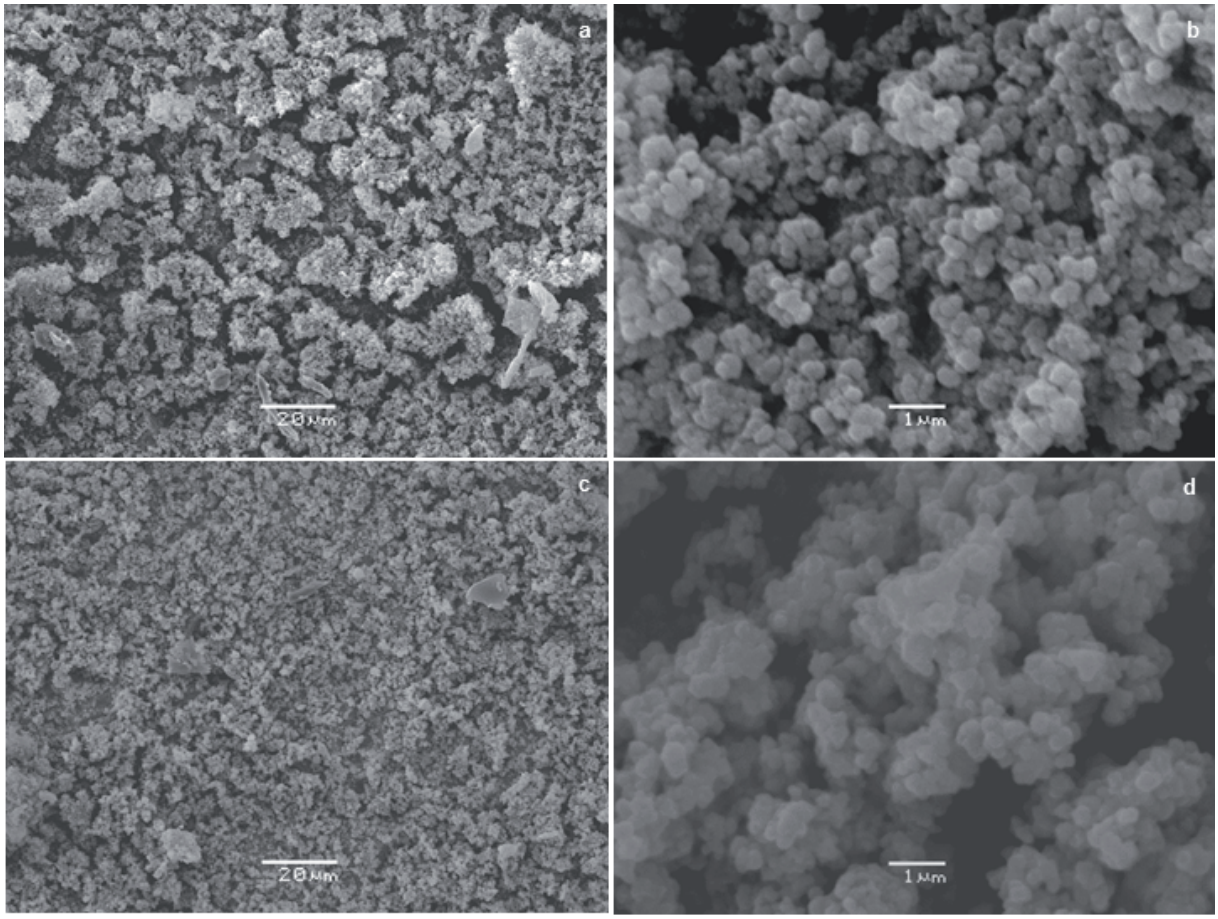

Fig. 2 SEM images of the TiO_2 photoelectrode sintered by a) and b) conventional furnace (600 ºC−1 h) and c) and d) induction heater (300 ºC−5 min).

samples, the differences between the reliefs are small when compared to the CF samples. This suggests that the film is more homogeneous with no significant aggregation in the fast sintering process. Figure 2d presents a slight improvement in the inter-particle interaction (IH samples) when compared with the film observed in Fig. 2b (CF samples).

In general, the surface morphology of the thin films fabricated using sol-gel technique displays a "cracked mud" structure, which seems to be a consequence of the shrinkage of the film during heat treatment [17-19]. The majority of the macrocracks or agglomerated powder islands exhibit a cracked-mud appearance. In addition, the pores observed in the SEM images have a regular shape, similar to cylindrical pores, which could have been formed during the burn out of polyethylene glycol (PEG) from the precursor-sol [20]. This type of morphology provides greater particle access to the liquid treated, yielding more active surface area for the photocatalytic process. A higher surface homogeneity is obtained via induction heating treatment, yielded a greater integrity and a higher stability due to the consolidation obtained between the particles. In addition, there are not effect of the temperature differences observed between the center of the samples and the outer area of the thin film, treated by the induction heater. The process seems to have a negligible effect on its surface morphology because no significant differences between those areas were identified. This is likely because the very fast sintering rate, lower temperature and short calcination time reduce the possibilities for generating different microstructures or morphologies along the thin film surface. The particle size and distribution in both film types are similar and sub-micrometric in size. The images in Fig. 2 illustrate that the samples exhibit nearly the same morphology after both calcination techniques. The differences are related to the agglomeration form of the particles over the film and the densification grade between the particles, making the coating more homogeneous for IH process, as was previously described.

To the best of our knowledge, this study represents the first time that this annealing technique has been used for this type of material. Others works, like the one presented by C. Mousty et al. [2] applied induction heating for the production of IrO_2/Ti electrodes using a 1 s pulse at 300-350 ºC. In our case, the home-made induction heater reached a temperature of 300 ºC in 1 min, providing good film homogeneity and with a substrate adherence slightly better than that obtained using the conventional furnace. Therefore, it was necessary to increase the sintering time to 5 min to improve the stability of the film.

The adhesion of TiO_2 thin film on the stainless steel substrate by sol-gel dip-coating is a difficult task. This is because no chemical bonding is obtained between the surface of the SS substrate and the titanium dioxide coating. Different

approaches have been used to improve the stability of the film. The best results have been produced using a high sintering temperature, approximately 700 to 900 ºC, or a long sintering time, i.e., 2 hours or more [8]. However, these processes typically reduce photocatalytic activity, during the transformation of anatase phase to rutile phase [17, 21]. Another method for enhancing the precursor-sol coating adhesion is adding polyethylene glycol PEG, which has a double function. It acts as a template particle rearrangement for a more homogeneous film on the substrate and it contributes to the mesoporous structure of the dioxide [8, 22]. In this case, the polyethylene glycol was added before the precursor sol were fabricated, which resulted in a more stable coating than the TiO_2 film without PEG.

The adhesion was confirmed by two methods of characterization, the scotch tape test (ASTM D3359) and the method used for P. Rodriguez et al. [17], which consists in immersing the samples on a beaker with distilled water at room temperature and at 80 ºC for 8 h, and then measuring the weight of the samples before and after the treatment. With the scotch method an adhesion around 85 % (T-IH) and 70 % (T-CF) were obtained, while with the immersion method, at both temperatures, a weight loss of 5 % (T-IH) and 10 % (T-CF) were observed. The stability of the thin film in a liquid media is important for the photocatalytic application. The obtained scotch tape result showed that an improvement of the mechanical resistance of the thin film is necessary, for both samples. The lower adhesion on T-CF film in comparison with the literature is due to the low sintering time used in this work.

3.1.3 Structural characterization of TiO_2 films

The anatase phase was confirmed for both sample types, and sintered for both methods. Figure 3 shows the XRD pattern of the films. It is possible to see rutile phase in this figure. In general, alkoxide precursor-sol with or without PEG generate rutile phase at 500 or 600 ºC [20, 21]. In this case, the rutile phase formation is promoted by induction heating at 300 ºC. The formation of a rutile phase was not expected for the fast sintering thin films using IH because the temperature reached is less than 500 ºC. However, the accelerated sintering mechanisms likely caused the formation of this stable phase at a lower temperature. In the other hand, it is demonstrated that a small quantity of rutile phase could help to the mechanism of photocatalysis, as TiO_2 Degussa P25 had demonstrated.

From this diffractogram path crystal size was measured using Scherrer equation. For TiO_2-IH sample the crystallite size was 15 nm and for TiO_2-CF 22 nm for the anatase phase.

To ensure the stability of the thin film, different coting cycles were studied. In a preliminary stage, 1 to 10 cycles were carried-out, the results showed that the one layer film presented a slight translucent surface with slight coloration from the iron oxide formed on the substrate surface during sintering, for both type of samples, with a low mechanical resistance. While for 10 cycles, the thin film showed the typical white color of titanium oxide with an enhancement of the mechanical stability. In Fig. 4a and 4b, it is shown that the thickness of the coating was 32.6 ± 1.20 μm and 47.77 ± 1.18 μm, for T-IH and T-CF respectively. From these images, it can be seen large pores from the surface of the film to the surface of the substrate. During the preparation of the sample for SEM images, in the cutting process, the samples lost part of the film. Comparing the thickness measured with the SEM images and the ones calculated from density measurements, the reduced thickness was about 10 %. The larger pores of T-IH sample is confirmed with the SEM image of the cross section of the film, these were filled with resin during metallurgy preparation.

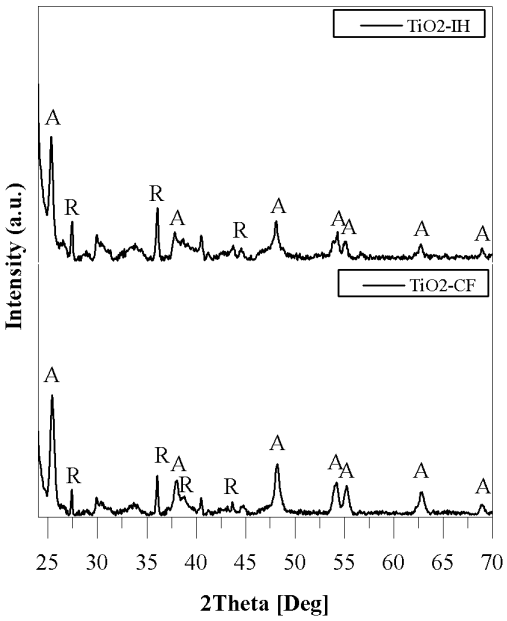

Fig. 3 XRD patterns of TiO_2 sintered by a conventional furnace (CF) and induction heating (IH).

3.2 Electrochemical characterization

3.2.1 Linear sweep voltammetry

Linear sweep voltammetry was performed in the dark and under illumination conditions for the electrodes in study, as shown in Fig. 5. In the dark, the TiO_2 (CF) electrode did not exhibit polarization currents at the applied potential, as is expected for this material. The titanium oxide film sintered with the induction heater exhibits a polarization current from the beginning of the applied potential. In particular, the induction heater provides more current than does the conventional furnace treatment. This could be due to a higher contact between the particles obtained by the sintering treatment with induction heating, as was reported in Section 3.1.2. Conversely, the current response under illumination was slightly higher for IH-samples than CF-samples.

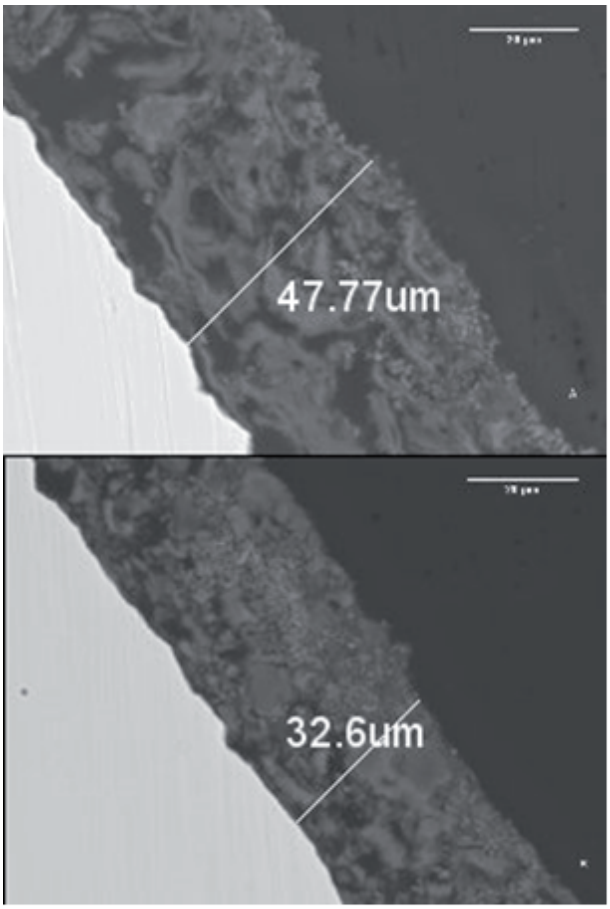

Fig. 4 SEM images of a) TiO_2-CF and b) TiO_2-IH for 10 cycles of dip-coating at 2 mm s-1 of withdraw rate and 1 min of holding time (1,85KX).

3.2.2 Electrochemical impedance spectroscopy

To study the electrical properties, of TiO_2 fabricated by the conventional furnace and induction heater, Electrochemical Impedance Spectroscopy were conducted in a frequency range of 100 kHz to 100 mHz under a DC applied potential of +0.2 $V_{Ag/AgCl}$. From the Nyquist plots (Fig. 7a), TiO_2-IH exhibits a lower impedance than TiO_2-CF, which indicates that the electron-transfer processes are improved. This is due to lowering of the recombination rate by obtaining a homogeneous surface, using a very fast sintering process, which reduces the charge-transfer resistance when the impedance is lower. In the inset of Fig. 7a, a small semicircle can be seen in the high frequency region. Previous studies have suggested that this is due to the resistance and capacitance of the coating (parallel configuration) [22]. Figure 6 illustrates the equivalent circuit (EC) selected to fit the data. Nir Baram and Yair Ein-Eli [22] employed a similar model, but with additional RC circuits parallel to the space charge capacitance and the charge transfer resistance, which in our case are denoted by CPE_2 and R_3, respectively. They based their EC on the Robert and Crowell models, where the equivalent circuit contains the solution resistance, the R-C_{dl} parallel circuit of the double layer and the R-C parallel circuit of the space charge with the disposition of R-C series circuits in parallel with the space charge transfer resistance. These correspond to discrete donor levels that can act as trapping levels or as recombination centers, depending on the frequency and potential applied. In our case, just one R-C pair was admitted in the equivalent circuit, and instead of capacitors, it was necessary to use constant phase elements due to the inhomogeneity of the system (pores, surface roughness, among other factors). The impedance of the constant phase element is

$$Z_{CPE} = \sigma\omega^{-n}\left[\cos\left(n\pi/2\right) - j\cdot\sin\left(n\pi/2\right)\right] \qquad (1)$$

Where σ is the CPE pre-factor, ω is the angular frequency ($\omega = 2\pi f$), n is the CPE exponent ($0 \leq n \leq 1$) and j is an imaginary number ($j = -1$). When n approaches 1, Z_{CPE} acts as a capacitor. If $n = 0.5$, it represents a Warburg impedance, and if $n = 0$, it represents a resistance [23].

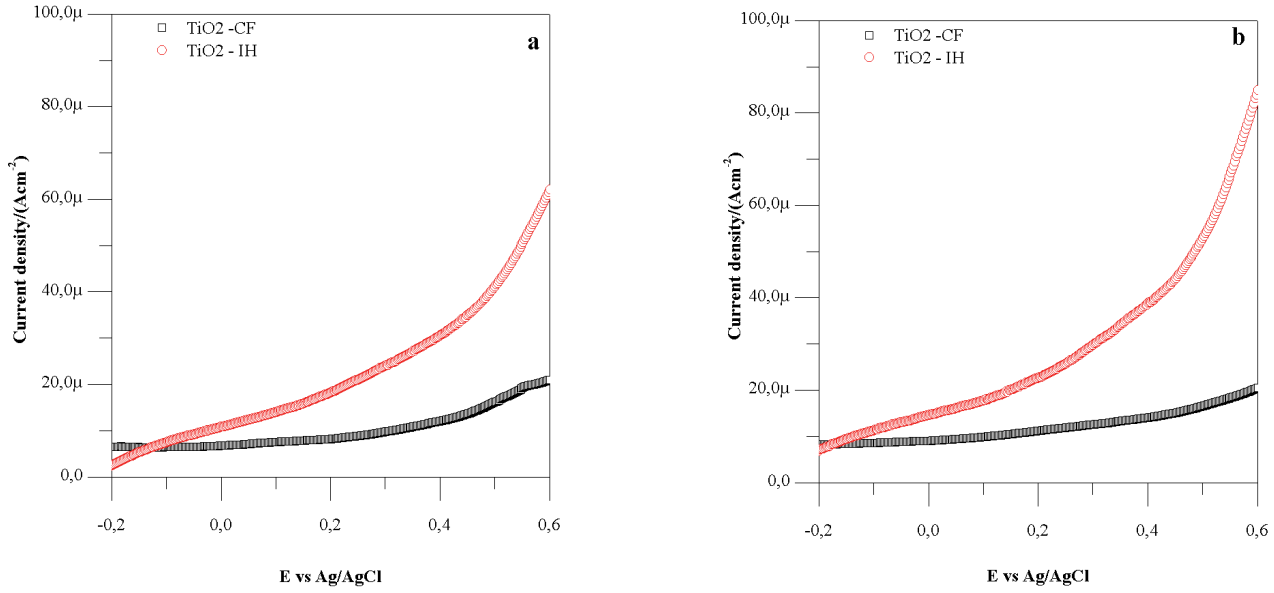

Fig. 5 Linear sweep voltammetry curves of all photoelectrodes: (a) in the dark and (b) under illumination. (a-TiO_2 conventional furnace (CF); b-TiO_2 induction heater (IH); Photoelectrode// Ag/AgCl // Pt// in 0.1 M K_2SO_4 pH=6.74.

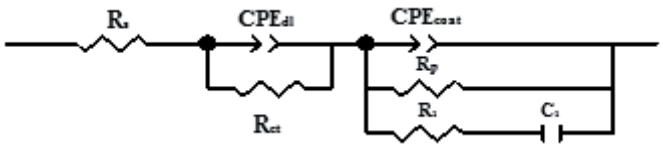

Fig. 6 Equivalent circuit

The almost linear form of the low-frequency portion of the Nyquist curve in Fig. 7 suggests that a diffusive capacitance phenomenon is occurring. This phenomenon is generally modeled as a Warburg impedance element in equivalent circuits and indicates that the electrodes have a high roughness and low surface homogeneity. However, an EC with this element was difficult to fit to the measured data. The results of the fitting model are represented by the solid line that connects the measured data, which are presented as symbols. Using the equivalent circuit mentioned above, the calculated EC parameters are listed in Table 1. As is generally observed in this type of analysis, the R_s is the solution resistance, with values presented in the same order. The electrode parameter results indicate that TiO_2-IH has a less porous layer, as demonstrated in the SEM image because the higher R_p (Porous resistance) value indicates a more compact layer.

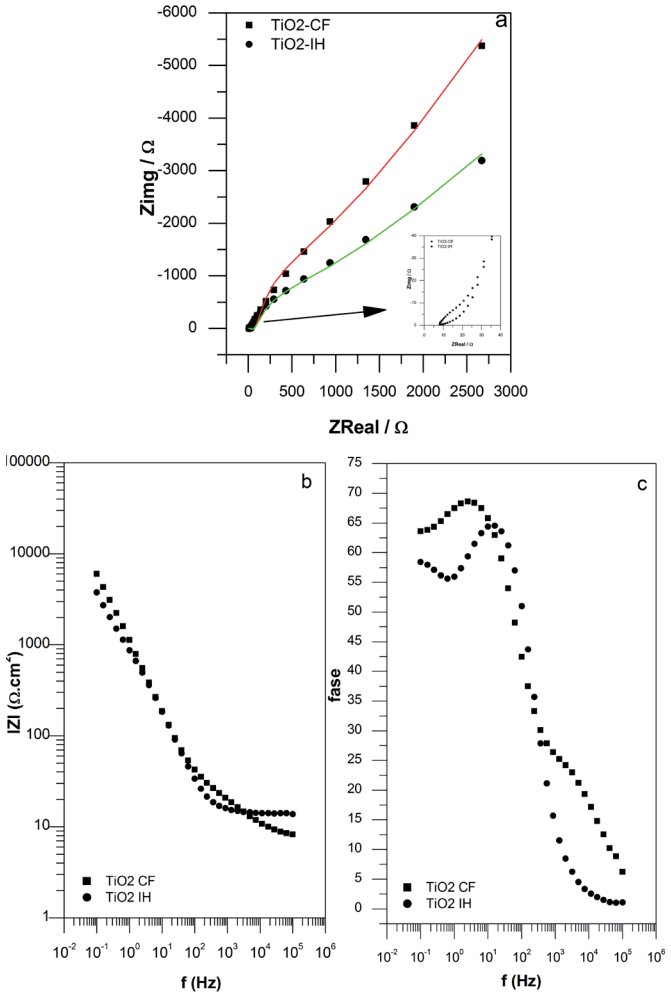

Fig. 7 Nyquist (a) and Bode (b) plots of TiO_2 conventional furnace (CF); TiO_2 induction heater (IH); Photoelectrode/ Ag/AgCl / Pt/ in 0.1 M K_2SO_4 pH=6.74.

Table 1 Data fitted from EIS analysis for the studied electrodes in dark conditions.

Sample	TiO_2-CF	TiO_2-IH
R_s [Ω.cm²]	7.432 ± 0.063	13.91 ± 0.057
CPE_{dl} [μF/cm²]	228.23 ± 3.48	430 ± 10.8
n_{dl}	0.79 ± 0.003	0.99 ± 0.08
R_{ct} [Ω.cm²]	37542 ± 1423.6	8157 ± 509.43
CPE_{coat} [μF/cm²]	295.5 ± 1.46	245 ± 28.9
n_{coat}	0.59 ± 0.009	0.76 ± 0.02
R_p [Ω.cm²]	239 ± 7.03	989.8 ± 15.4
R_1 [Ω.cm²]	20.99 ± 0.68	3.36 ± 0.76
C_1 [μF/cm²]	743.3 ± 15.6	15.3 ± 3.2

The R_{ct} and CPE_{dl} values are normally associated with the porous external layer of the electrode (high-frequency result in Nyquist plots). In addition, the n_{dl} values approach the unit value for all electrodes, which mean that CPE act as capacitors.

3.2.3 Mott-Schottky Analysis

Capacitance, carrier donor density and flat band potential are essential calculations reported using a Mott-Schottky analysis for semiconductor electrodes. The plots obtained for dark conditions ($1/Cs^2$ vs electrode potential) are presented in Fig. 8. Figure 8a, illustrates that the expected n-type semiconductor behaviors are obtained, but with higher capacitance values for the electrode sintered using the conventional furnace. The flat band, Ef_b, and donor density, N_D, calculated from the slope of the curve are reported in Table 2. Flat band parameters exhibited significant change, and the charge carrier densities of the titanium dioxide electrodes produced values in typical range described in the literature, ranging from 10^{16} to 10^{21} cm^{-3} [24]. Moon Su Kim et al. [25] reported Ef_b (vs Ag/AgCl) values for TiO_2 equal to the values obtained here when using the conventional furnace method. The annealing temperature, duration of the heat treatment, doping process and the physical characteristics, such as morphology and crystallinity, affect N_D and Ef_b values. Even the protocol measurement can affect the values, as was shown by M.C.K. Seller and E.G. Seebauer in their report [24].

Table 2 Flat Band Potential and Charge Carrier concentration of the studied electrodes via Mott-Schottky calculations.

Sample	TiO_2-CF	TiO_2-IH
N_D [cm^{-3}]	5.77 x 10^{19}	1.34 x 10^{21}
E_{fb} [$V_{vsAg/AgCl}$]	−0.58	−0.72

The improvement in the photocurrent is subjected to a higher donor density, N_D. Comparing sintering methods, the charge carrier density increases with induction heating and is correlated

with the shift of the flat band to a more negative value. The donor densities obtained are in agreement with the polarization current curves. In general, a larger carrier density is obtained by doping the titanium dioxide. Therefore, it was the fast sintering method that provided a higher N_D . The thinner film obtained could include more superficial defects that increase the donor density. Another possibility, which is more effective and has been reported in the literature, is lower sintering temperature used with the induction heater. This could create a higher oxygen vacancy on the film and enhance the quantity of N_D [23].

When the flat band shifted to a more negative value, the charge carrier density increased. Ilie Hanzu et al. [26] noted that Nernst-type law behavior is observed when the changes in the flat band potential of a quart of a volt generated an increment of donor density of 4 orders of magnitude. As reported in Table 2, a more negative flat band was obtained for the sample sintered by induction heating at 0.14 V, which resulted in a charge carrier density of 2 orders of magnitude higher.

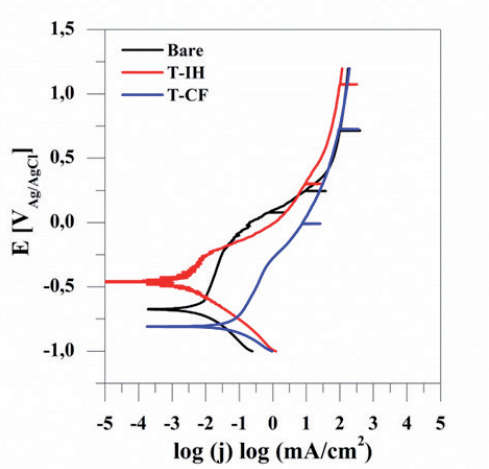

Fig. 9 Tafel curves for SS AISI304 bare and with coating, TiO_2 sintered by induction heater (T-IH) and conventional furnace (T-CF).

3.2.4 Corrosion measurements

Resistance to the environmental oxidation of the Stainless Steel substrate uncoated and coated with titanium dioxide, and sintered by induction heating and conventional furnace, were studied by polarization measurements with NaCl (3.5 wt%) [21, 27-30]. Tafel polarization curves (Fig. 9), showed that corrosion resistance has a dependency of the sintering technique, due to the effect of these processes on the coating morphology. The T-IH film presented lower corrosion potential and corrosion current density than bare substrate and T-CF sample, improving its corrosion resistance. As it was observed from SEM images of the surface morphology, the T-CF film showed a crack mud type surfaces with deeper and larger pores than T-IH film. This higher porosity contributed to a higher penetration of the electrolyte through the pores, reaching the surface of the substrate and reducing the corrosion resistance of the Stainless Steel. For both coating, polyethylene glycol (PEG) was added, and it is already know [20, 21] that its decomposition during sintering process generates porosity on the thin film. For photocatalysis, this porosity on the thin film form is necessary to reach a behavior near to the powder form, because this gives more active surface area of TiO_2 during pollutant degradation process.

The corrosion parameters calculated by Tafel's law are shown in Table 3, the corrosion current density of T-CF sample is higher than AISI304, and this could be due to chemical treatment performed on the substrate before coating, in which it was increased the roughness of the surface for a better anchoring of the film. However, this treatment reduces the self-passivation of the stainless steel which gives a higher corrosion problem to the T-CF thin film than for the pure substrate. While, even when T-IH samples have some porosity that allow the electrolyte reached the Stainless Steel substrate, this porosity could be smaller and closer in the first layers of the film, improved by the temperature obtained within the surface of the substrate to sinter the film with the induction heater, improving at the end the corrosion resistance of the stainless steel.

On the other hand, during and after photocatalytic degradation of MB, no corrosion, of both coated films was observed. However, a further fully corrosion characterization it is necessary.

Table 3 Corrosion parameters of bare and TiO_2 coated stainless steel in 3.5 wt% of NaCl determined by Tafel extrapolation method.

Samples	SS304	TiO_2IH	TiO_2CF
i_{corr} [μA/cm²]	30.50	15.16	53.62
E_{corr} [mV vs Ag/AgCl]	−664.58	−449.49	−768.72
b_a [mV/dec]	709.24	228.5	690.03
$-b_c$ [mV/dec]	229.96	165.56	171.43
R_p [Ω*cm²]	2509.28	2749.71	1111.98
OCP [mV vs Ag/AgCl]	−547.56	−406.87	−776

3.3 Photo-degradation of Methylene Blue

The electrochemical properties measured reveal that TiO_2 sintered by induction heating (T-IH) has the potential to better oxidize toxic organic components, such as the azo dye used in this study. The photocatalytic oxidation of 0.01 M of methylene blue (MB) was performed in a reactor, as described in Section 2.5, with UV illumination.

The change in the UV-Vis absorbance of MB is shown in Fig. 10. The pH of the solution was set to 10, which previous studies [31-33] report to be the best condition for achieving higher methylene blue degradation due to the high TiO_2 adsorption. This adsorption is promoted by a negative charge on the catalyst surface, which is obtained in a basic medium [31, 33, 34]. Regarding the adsorption-desorption equilibrium of methylene blue on the photocatalysts, the first solution sample was obtained after 2 h in the dark and the UV illumination of the systems began.

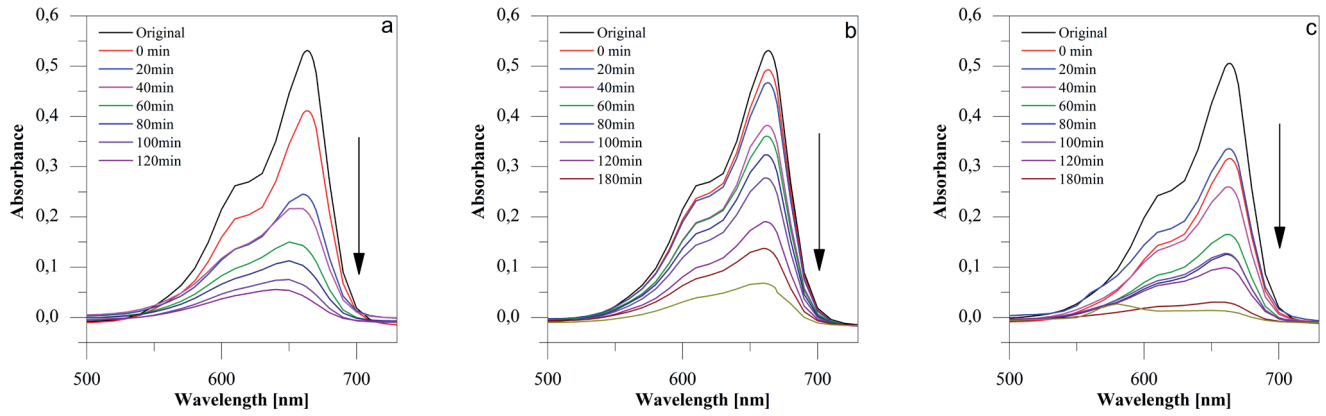

Fig. 10 UV-Vis Absorbance spectra of the methylene blue 0.01 M solution at a pH10 during photocatalytic degradation under UV illumination using a) TiO_2 sol-gel powder, b) TiO_2-CF and c) TiO_2-IH over 4 h

The degradation rate was analyzed every 20 min for the first 2 h and then two more aliquots were withdrawn at the third and fourth hour of illumination. Figure 10c illustrates that the T-IH MB absorbance value in the dark decreased more than the value for the T-CF electrode. This is due to the higher adsorption capability of the dye observed under the first conditions (See the Fig.10c). This could be due to the more regular and smaller surface morphology obtained by the induction heating treatment, as was observed in the SEM image. This allowed the T-IH electrode surface to act as sponge, improving the contact between the channels of TiO_2 thin film and the organic molecules of the MB dye. Nevertheless, no degradation was observed in the first 20 min of UV illumination and some of the organic molecules adsorbed by the electrode were seemingly released to the solution, which resulted in an increase of concentration. Then, degradation began to occur at a higher rate than the T-CF oxidation.

The rate of variation of the concentration is shown in Fig. 11. The MB solution without a catalyst exhibited a slight UV light degradation, as reported in the literature for this type of azo dye [31-33]. Therefore, this does not affect the performance of the photocatalysts and it may be negligible. The faster and greater degradation of MB by T-IH samples is possibly due to a higher surface area of the thin film surface morphology, as was mentioned in Section 3.2.1. It may also be due to an advanced transfer of the charge carrier formed during UV illumination, which is due to improved particle interconnections obtained via the induction heating sintering method, as observed in SEM image (Fig. 2d). In this plot, it is possible to see that the T-IH electrode surface exhibited a higher absorption than the TiO_2 powder in the dark. The color of the MB solution changes to colorless after 180 min for the T-IH sample, as is observed in Fig. 11b.

The T-IH sample degradation reached approximately 93 %, after 240 min and approximately 80 % for the T-CF sample. This suggests that an improved photocatalytic activity was achieved with the new annealing treatment, at least for the consolidation of this type of coating. Titanium dioxide powder synthesized using the same precursor-sol , with 2 g of PEG, and sintered at 600 ºC for 1 h was used as a photocatalysis control parameter. It reached 90 % of degradation after 120 min for 0,01 M MB, pH 10, with 1 g/L of catalyst. The catalyst powder sintered at 300 ºC yielded a large quantity of ashes due to the amount of PEG added. This resulted in a color change of the methylene blue solution during the 2 h of dark adsorption, transforming the solution from blue to a dark brown (the color of the powder catalyst). The UV-Vis spectrophotometry study of this solution, after removing the photo-catalyst powder by centrifugation, exhibited a degradation of 90 %. More studies will be necessary to further understand this powder behavior. The degradation rate of the electrode in the study followed a first-order law, (see Fig. 12) and the values obtained are presented in Table 4.

Table 4 Degradation rate of the titanium dioxide electrode in the study.

Sample	k(10^{-3} min^{-1})
TiO_2 p	15.67
T-CF	6.93
T-IH	9.01

In this study, we demonstrated that the use of a faster sintering method, such as induction heating, can produce a homogeneous TiO_2 thin film structure on stainless steel substrate, with good photocatalytic performance for the degradation of methylene blue. Although the results suggest an improved photodegradation efficiency of azo dye using UV illumination, further study is needed involving the fabrication of TiO_2 doped or in a composite materials with visible light activation.

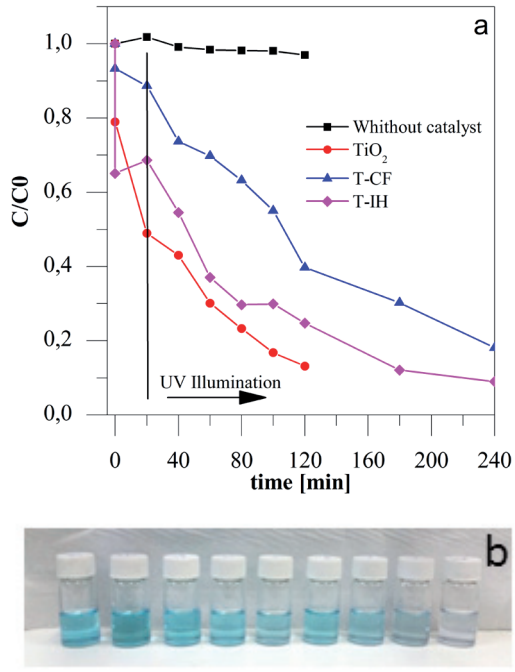

Fig. 11 a) Concentration variation of the methylene blue during photocatalytic degradation in 4 h. b) Discoloration photo of MB 0.01 M, pH 10 for the T-IH sample.

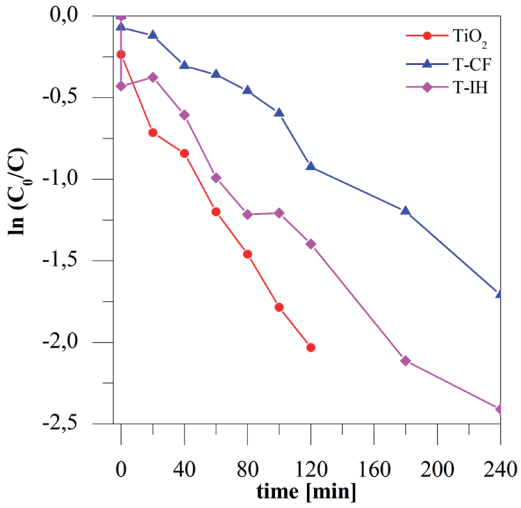

Fig. 12 Kinetic simulation curves of MB photocatalytic degradation with TiO_2 powder, T-IH and T-CF electrodes.

4 Conclusions

A photocatalytic TiO_2 thin film on stainless steel was obtained using an induction heating method as a thermal treatment. Based on our results, we can conclude that it is a reliable technique for obtaining more homogeneous and stable surface morphologies of sol-gel thin film, compared with conventional furnaces. The method also takes less time, 5 min, and uses a lower temperature (300 ºC instead of the 600 ºC and 1 h on the CF). Therefore, it represents a scalable and low-cost method. The induction heating samples exhibited a higher charge carrier density with a more negative flat band and generated more dye absorption during the degradation analysis. This resulted in a higher photocatalytic activity than conventional furnace electrodes. A 90 % degradation and discoloration was reached for T-IH samples, as compared to 80 % degradation for the T-CF electrode obtained over 240 min. Therefore, more studies are required to improve the photocatalytic activity with respect to the TiO_2 powder obtained from the same sol-gel with 2 g of PEG sintered at 600 ºC for 1 h, which reached 90 % degradation and a MB discoloration in 120 min. The small temperature differences from the center of the electrodes to the outer portions, during induction heating, did not affect the photocatalytic activity of the samples. Also, corrosion resistance was improved using induction heating at a sintering technique, by reducing the porosity obtained during PEG decomposition and by enhancing the homogeneity of the surface film morphology. The results suggest reproducibility. Further studies with TiO_2 doping or other composites with elements that provide photocatalytic activity in visible light will be performed.

Acknowledgements

The authors would like to thank CONICYT-Chile for providing financial support by the project FONDECYT Nº 3130669. Also thanks to VRIEA-PUCV and EIE-PUCV photometry laboratory for their collaboration.

References

[1] Xu, H., Li, A., Cheng, X. "Electrochemical Performance of Doped SnO2 Coating on Ti Base as Electro-oxidation Anode." *International Journal of Electrochemical Science*. 6, pp. 5114-5124. 2011. URL: http://www.electrochemsci.org/papers/vol6/6115114.pdf

[2] Mousty, C., Fóti, G., Comninellis, Ch., Reid, V. "Electrochemical behaviour of DSA type electrodes prepared by induction heating." *Electrochimica Acta*. 45(3), pp. 451-456. 1999. DOI: 10.1016/S0013-4686(99)00273-X

[3] Ochuma, I. J., Osibo, O. O., Fishwick, R. P., Pollington, S., Wagland, A., Wood, J. J., Winterbottom, M. "Three-phase photocatalysis using suspended titania and titania supported on a reticulated foam monolith for water purification." *Catalysis Today*. 128(1-2), pp. 100-107. 2007. DOI: 10.1016/j.cattod.2007.05.015

[4] Giornelli, T., Löfberg, A., Bordes-Richard, E. "Preparation and characterization of VOx/TiO2 catalytic coating on stainless steel plates for structured catalytic reactors." *Applied Catalysis A: General*. 305(2), pp. 197-203. 2006. DOI: 10.1016/j.apcata.2006.03.024

[5] Marin, E., Lanzutti, A., Lekka, M., Guzman, L., Ensinger, W., Fedrizzi, L. "Chemical and mechanical characterization of TiO2/Al2O3 atomic layer depositions on AISI 316 L stainless steel." *Surface & Coatings Technology*. 211, pp. 84-88. 2011. DOI: 10.1016/j.surfcoat.2011.08.026

[6] Wei, C.-H., Tang, X.-H.., Liang, J.-R., Tan, S.-Y. "Preparation, characterization and photocatalytic activities of boronand cerium-codoped TiO2." *Journal of Environmental Sciences*. 19(1), pp. 90-96. 2007. DOI: 10.1016/S1001-0742(07)60015-1

[7] Baiju, K.V., Periyat, P., Krishna Pillai, P., Mukundan, P., Warrier, K. G. K., Wunderlich, W. "Enhanced photoactivity and anatase thermal stability of silica–alumina mixed oxide additives on sol–gel nanocrystalline titania." *Materials Letters*. 61(8-9), pp. 1751-1755. 2007. DOI: 10.1016/j.matlet.2006.07.124

[8] Chen, Y., Dionysiou, D. D. "A comparative study on physicochemical properties and photocatalytic behavior of macroporous TiO2-P25 composite films and macroporous TiO2 films coated on stainless steel substrate." *Applied Catalysis A: General*. 317(1), pp. 129-137. 2007. DOI: 10.1016/j.apcata.2006.10.025

[9] Jie, T., Jie, D., Xiang, D., Hong, Z., Hai-jun, T. "Enhanced photocatalytic properties of hierarchical nanostructured TiO2 spheres synthesized with titanium powders." *Transaction of Nonferrous Metals Society of China*. 22(8), pp. 2049-2056. 2012. DOI: 10.1016/S1003-6326(11)61427-1

[10] Sriwong, Ch., Wongnawa, S., Patarapaiboolchai, O. "Rubber sheet strewn with TiO2 particles: Photocatalytic activity and recyclability." *Journal of Environmental Sciences*. 24(3), pp. 464-472. 2012. DOI: 10.1016/S1001-0742(11)60794-8

[11] Li, Ch., Han, J., Zhang, Z., Gu, H. "Preparation of TiO2-Coated Al2O3 Particles by Chemical Vapor Deposition in a Rotary Reactor." *Journal of the American Ceramic Society*. 82(8), pp. 2044-2048. 1999. DOI: 10.1111/j.1151-2916.1999.tb02038.x

[12] Morks, M.F., Akimoto, K. "The role of nozzle diameter on the microstructure and abrasion wear resistance of plasma sprayed Al2O3=TiO2 composite coatings." *Journal of Manufacturing Processes*. 10(1), pp. 1-5. 2008. DOI: 10.1016/j.jmapro.2008.10.001

[13] Tian, W., Wang, Y., Yang, Y., Li, Ch. "Toughening and strengthening mechanism of plasma sprayed nanostructured Al2O3–13 wt.%TiO2 coatings." *Surface & Coatings Technology*. 204(5), pp. 642-649. 2009. DOI: 10.1016/j.surfcoat.2009.08.045

[14] Verran, J., Packer, A., Kelly, P., Whitehead, K. A. "Titanium-coating of stainless steel as an aid to improved cleanability." *International Journal of Food Microbiology*. 141(Supplement), pp. S134–S139. 2010. DOI: 10.1016/j.ijfoodmicro.2010.04.027

[15] Yang, H., Sun, Y., Shen, J., Hu, S., Zhao, Q., Jia, X., Zhang, J. "Microstructure and Properties of Fe-Based Coating on Column Surface Formed by High Frequency Induction Cladding." *Journal of Surface Engineered Materials and Advanced Technology*. 2(1), pp. 40-43. 2012. DOI: 10.4236/jsemat.2012.21007

[16] Bay, F., Labbe, V., Favennec, Y., Chenot, J. L. "A numerical model for induction heating processes coupling electromagnetism and thermomechanics." *International Journal for Numerical Methods in Engineering*. 58(6), pp. 839-867. 2003. DOI: 10.1002/nme.796

[17] Rodríguez, P., Meille, V., Pallier, S., Al Sawah, M. A. "Deposition and characterisation of TiO2 coatings on various supports for structured (photo) catalytic reactors." *Applied Catalysis A: General*. 360(2), pp. 154-162. 2009. DOI: 10.1016/j.apcata.2009.03.013

[18] Carlesi Jara, C., Salazar-Banda, G. R., Schrebler Arratia, R., Silva Campino, J., Irrazábal Aguilera, M. "Improving the stability of Sb doped Sn oxides electrode thermally synthesized by using an acid ionic liquid as solvent." *Chemical Engineering Journal*. 171(3), pp. 1253-1262. 2011. DOI: 10.1016/j.cej.2011.05.039

[19] Lassali, T. A. F., Boodts, J. F. C., Bulhões, L. O. S. "Effect of Sn-precursor on the morphology and composition of Ir0.3Sn0.7O2 oxide films prepared by sol-gel process." *Journal of Non-Crystalline Solids*. 273(1-3), pp. 129-134. 2000. DOI: 10.1016/S0022-3093(00)00152-6

[20] Balasubramanian, G., Dionysiou, D. D., Suidan, M. T., Baudin, I., Laîné, J. "Evaluating the activities of immobilized TiO2 powder films for the photocatalytic degradation of organic contaminants in water." *Applied Catalysis B: Environmental*. 47(2), pp. 73-84. 2004. DOI: 10.1016/j.apcatb.2003.04.002

[21] Ćurković, L., Otmačić Ćurković, H., Salopek, S., Majić Renjo, M., Šegota, S. "Enhancement of corrosion protection of AISI 304 stainless steel by nanostructured sol–gel TiO2 films." *Corrosion Science*. 77, pp. 176-184. 2013. DOI: 10.1016/j.corsci.2013.07.045

[22] Baram, N. Ein-Eli, Y. "Electrochemical Impedance Spectroscopy of Porous TiO2 for Photocatalytic Applications." *Journal of Physical Chemestry C*. 114(21), pp. 9781-9790. 2010. DOI: 10.1021/jp911687w

[23] Gelderman, K., Lee, L., Donne, S. W. "Flat-Band Potential of a Semiconductor: Using the Mott–Schottky Equation." *Journal of Chemical Education*. 84(4), pp. 685-688. 2007. DOI: 10.1016/j.apcata.2006.10.025

[24] Sellers, M. C. K., Seebauer, E. G. "Measurement method for carrier concentration in TiO2 via the Mott–Schottky approach." Thin Solid Film. 519(7), pp. 2103-2110. 2011. DOI: 10.1016/j.tsf.2010.10.071

[25] Kim, M. S., Jo, W. J., Lee, D., Baeck, S., Shin, J. H., Lee, B. Ch. "Enhanced Photocatalytic Activity of TiO2 modified by e-beam Irradiation." *Bulletin of the Korean Chemistry Society*. 34(5), pp. 1397-1400. 2013. DOI: 10.5012/bkcs.2013.34.5.1397

[26] Hanzu, I., Djenizian, T., Knauth, P. "Electrical and Point Defect Properties of TiO2 Nanotubes Fabricated by Electrochemical Anodization." *The Journal of Physical Chemistry C*. 115(13), pp. 5989-5996. 2011. DOI: 10.1021/jp1111982

[27] Shanaghi, A., Sabour, A. R., Shahrabi, T. Aliofkhazraee, M. "Corrosion protection of Mild Steel by applying TiO2 nanoparticles coating via sol-gel method." *Protection of Metals and Physical Chemestry of Surfaces*. 45(3), pp. 305-311. 2009. DOI: 10.1134/S2070205109030071

[28] Volentiru, E., Nyár, M., Szabó, G., Hórvölgyi, Z., Mureşan, L. M. "Silica sol – gel protective coatings against corrosion of zinc substrates." *Periodica Polytechnica Chemical Engineering*. 58(Sup). pp. 61-66. 2014. DOI: 10.3311/PPch.7302

[29] Chen, S., Cai, Y., Zhuang, C., Yu, M., Song, X., Zhang, Y. "Electrochemical behavior and corrosion protection performance of bis-[triethoxysilylpropyl] tetrasulfide silane films modified with TiO_2 sol on 304 stainless steel." *Applied Surface Science*. 331, pp. 315-326. 2015. DOI: 10.1016/j.apsusc.2015.01.008

[30] Szabó, G., Volentiru, E., Hórvölgyi, Z., Mureşan, L. M. "Protective TiO2 Coatings Prepared by Sol-Gel Method on Zinc." *Studia UBB Chemia*. 60(3), pp. 225-235. 2015. URL: http://chem.ubbcluj.ro/~studiachemia/docs/Chemia32015.pdf

[31] Salehi, M., Hashemipour, H., Mirzaee, M. "Experimental Study of Influencing Factors and Kinetics in Catalytic Removal of Methylene Blue with TiO2 Nanopowder." *American Journal of Environmental Engineering*. 2(1), pp. 1-7. 2012. DOI: 10.5923/j.ajee.20120201.01

[32] Li, J., Zheng, L., Li, L., Xian, Y., Jin, L. "Fabrication of TiO2/Ti electrode by laser-assisted anodic oxidation and its application on photoelectrocatalytic degradation of methylene blue." *Journal of Hazardous Materials B*. 139(1), pp. 77-78. 2007. DOI: 10.1016/j.jhazmat.2006.06.003

[33] Tayade, R. J., Sivakumar Natarajan, T., Bajaj, H. C. "Photocatalytic Degradation of Methylene Blue Dye Using Ultraviolet Light Emitting Diodes." *Industrial & Engineering Chemistry Research*. 48(23), pp. 10262-10267. 2009. DOI: 10.1021/ie9012437

[34] Bubacz, K., Choina, J., Dolat, D., Morawski, A. W. "Methylene Blue and Phenol Photocatalytic Degradation on Nanoparticles of Anatase TiO2." *Polish Journal of Environment Study*. 19(4), pp. 685-691. 2010. URL: http://www.pjoes.com/pdf/19.4/685-691.pdf